

## **Effect of Age on Healthy Human Nasal Airflow: A Computational Analysis**

**Chih Fang Lee, Fong Sheng Su, Jie Yinn Chan and Parvathy Rajendran\***

*School of Aerospace Engineering, Universiti Sains Malaysia,  
Engineering Campus, 14300 Nibong Tebal, Malaysia.*

*\*Corresponding Author*

### **Abstract**

The effect of age on healthy human nasal airflow along the entire nasal cavity has been investigated. A Malaysian 5-years-old female child was selected, and computational fluid dynamic (CFD) was implemented to develop and perform numerical analysis, in order to provide clear visualization of nasal airflow, and simultaneously, to allow the comparison with other models – male child and female adult model from previous works. This comparison includes nasal geometry, cross-sectional area, pressure drop, average velocity magnitude, velocity contours as well as velocity vectors and streamlines along the nasal cavities. The Malaysia female child model exhibited a narrower and thinner nasal passageway, and also shorter turbinates region when comparing with other two models. Despite of this, a general trend was observed for the cross-sectional area and average velocity magnitudes profiles of the airways along the axial distance. Besides, pressure drop, also known as breathing resistance was found decreases as the age increases. Furthermore, in child, the flow field was noticed more concentrated centrally as the airstream is developing. The vortices were also found more prevalent in the upper olfactory region and just posterior to the nasal valve. Based on these evaluations, age is proven to provide impact on healthy human nasal airflow.

**Keywords** - Human Nasal, Nasal Airflow, Nasal Cavity, CFD, Respiratory System.

### **I. INTRODUCTION**

The human nasal cavity is a vital component to the respiratory system as it coordinates the environmental air before entering the respiratory system. There are three major functional roles of the nasal cavity – filtration, air-conditioning and lastly, olfaction. Nasal cavity acts as the front line defender of the internal respiratory organs such as

lung towards the foreign air-borne particles which are varying in sizes. The foreign air-borne particles which exceed certain size, greater than  $5\mu\text{m}$  are trapped on the ciliated mucosa, which will then be swallowed or expelled [1]. Only small particles, less than  $2\mu\text{m}$  are permitted to proceed to the lower nasal airways. Moreover, nasal cavity is also vital to the human respiratory system in term of air-conditioning of the inhaled air.

In order to protect the human respiratory system from extreme conditions, inhaled air is humidified and warmed to nearly alveolar conditions (at similar temperature as body and fully saturated with water vapour), a condition which is compatible to the human internal respiratory organs [2]. This process is occurred throughout the turbinate region which is covered by moist nasal mucosa, until reaching the posterior end of the nasal cavity, known as nasopharynx. Human nasal cavity also takes part in olfaction or in other words, sense of smell. Olfaction greatly relies on the sensory receptors known as olfactory epithelium, which is located on the top of the nasal cavity. This sensory receptors respond to airborne chemicals and thus enable human to differentiate the odour of various substances such as food.

The anatomy and physiology of the human nasal cavity is quite complicated as it involves three-dimensional geometry. In general, nasal cavity is mainly composed of four regions, namely vestibule, nasal valve, nasal turbinate and nasopharynx [3]. As shown in Fig 1, the nasal cavity is first divided into 2 symmetrically nasal airways by the nasal septum. Then, the airways narrow at the nasal valve, a region with the smallest cross-sectional area. The cross-sectional area of the nasal passageways next increases again at the end of the nasal valve or the beginning of the turbinate region (inferior, middle and superior turbinate).

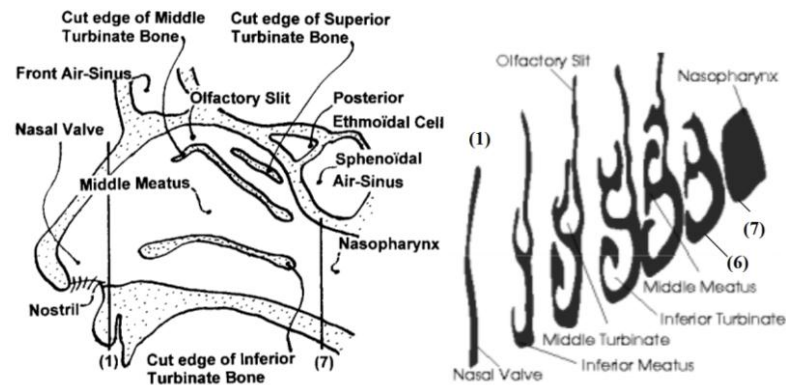


**Figure 1:** Nasal anatomy – Right Nasal View (a) Sagittal and (b) Geometry [4]

As mentioned earlier, this region is fully covered with moist nasal mucous layer and cilia for both filtration and air-conditioning purposes. The mucous layer is made of epithelium and lamina propria, which varies in thickness and features based on location and its capability in the nose [5]. Finally, the segregated nasal airways merge at the

posterior region of the nasal cavity, forming nasopharynx. In addition to the nasal cavity, there four extra air-filled lumens – paranasal sinuses which are connected with the air in the nasal airways [6].

CFD is a numerical simulation application that visualized the flow parameters such as velocity, pressure, vector, streamline and vorticity under variation flow conditions [7]. It has been proven in previous studies to be reliable in providing essential nasal information such as nose physiology, patho-physiology of normal breathing and also the flow patterns or behaviours across the nasal cavities (left and right nasal cavities) [8]. Since the advent of CFD in the late of 1960s, studies on the human nasal airflow regime have been conducted extensively. CFD has been widely utilized to analyse the nasal airflow which is troublesome to be performed through objective measurement approaches due to the complex human nose structure.

Besides, these researches were done in order to understand better various flow factors in the human nasal cavity, so that the rhinologist can implement advanced technology to overcome the technical difficulties of determining the exact diseases occurred on the patients. As a result, appropriate nasal surgery can be selected and performed towards a particular disease, greatly reducing the risk of surgery carried out. Moreover, this technology is also developed to replace rhinomanometry and acoustic rhinomanometry due to their poor accuracy, as measuring the precise velocity of the airflow and evaluating the local nasal resistance in every section of the nasal cavity have proven to be hard by using these two methods [9]. Further driven by the ever increasing demand, the analysis of nasal airflow in the human respiratory system became much more indispensable.

In this research, a healthy nasal cavity for a Malaysian female child has be developed (geometrical modelling), meshed and analysed using CFD. The data obtained will then be further compared and discussed with the male child and female adult nasal cavity model. The purpose of doing so is to study and understand the effect of age on the airflow in nasal cavity. Lack of available information in literature regarding child models encourages this research to be done, to provide good new addition to the current scientific knowledge. Besides, child model should be studied independently as data obtained from adult model will not be accurate due to the huge geometrical difference.

## **II. MATERIALS AND METHODS**

In recent years, there have been increasingly wide and deep applications of the CFD technique in investigating the airflow characteristics in the human nasal cavity due to the rapid development of computer resources, and hence its correlation with the symptoms and functions of the human nose [2], [10]–[14]. Majority of these studies used a combination of different software (e.g. MIMICS, AMIRA, CATIA, SOLIDWORK, GAMBIT, HYPERMESH, FLUENT and ANSYS) to produce and run simulation on the numerical nasal cavity models. In this study, a total of four software – MIMICS, CATIA, ANSYS Meshing and FLUENT were used to complete the analysis.

The methodology can be divided into three major sections – reconstruction of three-dimensional (3D) human nasal cavity, followed by volume meshing of geometry and lastly, computational analysis. The first part of methodology involved 3D model reconstruction of human nasal cavity from two-dimensional (2D) CT scans of a 5-years-old healthy female child nasal cavity that were obtained from Advanced Medical Dental Institute (AMDI), Universiti Sains Malaysia. The CT scans were transferred into MIMICS (Materialise, USA) to generate a 3D model of the nasal cavity. Three types of image – axial, coronal and sagittal with different orientations were acquired from MIMICS as shown in Fig 2(a). However, only axial images were considered and utilized in this study, to develop the human nasal cavity.

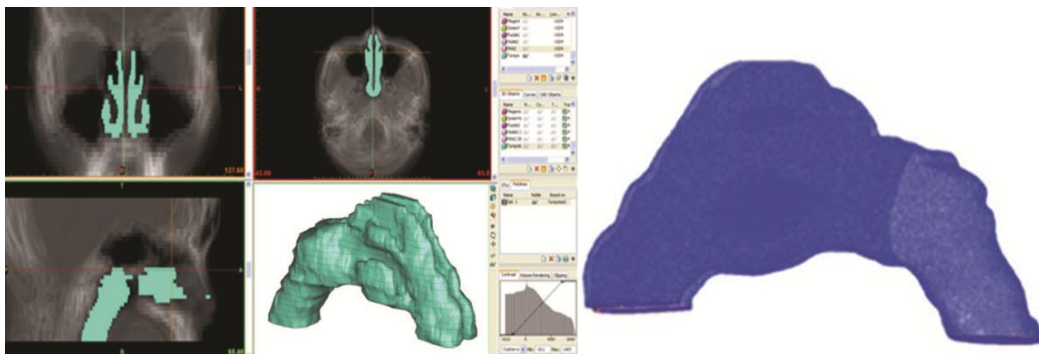


**Figure 2:** (a) Generation of axial, sagittal and coronal image in Mimics (b) Meshing of 3D geometry [15]

Unlike other directions, axial images are able to provide a clearer visualization towards the intricate geometry of the human nasal cavity, such as nasal turbinate. Several functions in MIMICS such as thresholding, defining and editing the masks (both 2D and 3D) were used to ease the generation of the model. Purpose of thresholding in MIMICS is to separate the pixels of desired region from the rest of the image [6]. In this case, by locating the thresholding span between -1024 and -951, pixels of the nasal airways (negative model) were selected and isolated from the others, and then forming a new mask.

The mask was next edited to remove unwanted regions and also to create precise airways morphology. Thereafter, another function known as Boolean Operation was also implemented to eliminate paranasal sinuses. The sinuses were deemed to have negligible impact on the gross airflow patterns due to small openings (ostia) with minimal cross-sectional area [16]. The 3D polylines data (IGES file) from MIMICS were then imported to CATIA V5 to polish the rough and uneven surfaces, and to trim the undesired geometries such as corrupted triangles, duplicated triangles, non-manifold edges and non-manifold vertices. Then, surfaces were generated with appropriate mean surface deviation and surface detail. Lastly, hollow surfaces model was converted into a closed surface fully solid volume and saved as STEP file for meshing purposes in ANSYS meshing.

Secondly, the methodology is focused on the meshing of the geometry. ANSYS meshing was the computer software used in this study to generate 3D meshes for the nasal cavity models. Due to complexity of nasal cavity morphology and also the narrowness of the nasal airways, some of the elements could be highly distorted, collapsed or linked together in wrong pattern, e.g. elements connected in T-shape (elements that belong to two isolated volumes sharing one edge). Hence, in order to repair such defected elements and produce high quality mesh, the geometry clean-up function in ANSYS Meshing was applied to fix the undesired geometries such as short edges, small and large angles, and small surfaces. After the completion of the clean-up action, volume meshing of the nasal cavity was performed as shown in Fig 2(b).

Both the inlet and outlet were also set via boundary type specification function; where inlet as the mass flow inlet while outlet as the outflow. Lastly, the mesh was exported as MSH file to ANSYS FLUENT. Generating the best suited mesh is the foundation of computational simulation in order to obtain an accurate and efficient solution and thus, the grid independence study was performed with unstructured tetrahedral meshing ranging from approximately 50000 to 150000 elements. The outcome showed that the grid dependency study resulted in an optimized meshing of 135185 elements and the computational results are validated with the pressure drop obtained from Xi et al. [17] and Lee et al. [15] as shown in Fig 3.

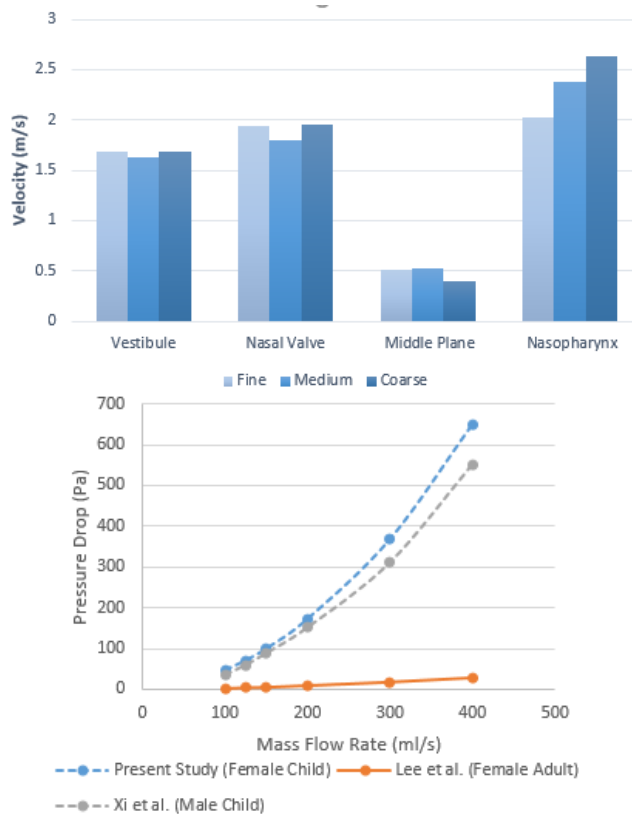


**Figure 3:** (a) Mesh dependency study at mass flow rate of 125 mL/s and (b) Pressure drop versus mass flow rate

Finally, the last part of this methodology involved running the analysis and analyzing the results. The numerical simulation was performed via finite volume method provided by ANSYS FLUENT Version 16.0. The simulation was based on the Navier-Stokes equations which govern the general three-dimensional fluid flow. In general, this phase can be divided into three stages – pre-processing, processing and post-processing. Pre-processing is the stage in which assumptions and boundary conditions are defined before proceeding to the simulation.

In this research, several assumptions were made to replicate a real human nasal cavity conditions. The airflow was assumed to be incompressible with constant density,  $1.225\text{kg}/\text{m}^3$  throughout the entire nasal cavity model [18], [19] and thus, pressure-based solver was implemented instead of density-based solver, which is typically the solution for the incompressible flow [3], [20]. Besides, the second order upwind solution method was applied to further improve the accuracy of the solution. Moreover, other suppositions such as steady airflow, isothermal flow, smooth rigid nasal wall, constant geometry, insignificant nasal hair effects and negligible gravitational effects were also made [9], [18], [21]–[24]. The boundary conditions were defined according to the previous researches.

The nasal wall was assumed to be rigid, with no slip shear condition, and the effects of mucous were assumed to be negligible as it is too thin to provide significant influences towards the airflow [9], [19], [25], [26]. The nostril inlet was defined previously as mass flow inlet, and the outlet at nasopharynx as the outflow boundary condition. Any backflow at the outlet was assumed to be at  $32.6\text{ }^\circ\text{C}$  and 100% relative humidity as imposed in ANSYS FLUENT [27]. Due to lack of information regarding the exact mass flow rate of laminar and turbulent nasal airflow, hence, in this work, the mass flow rate used was based on the previous researches as shown in

Table 1 [8], [9], [20], [25], [26], [28]. The airflow was treated as laminar for flow rate up to 250ml/s. Meanwhile, beyond that, all the flow was considered as turbulent.

**Table 1:** Mass flow rate for laminar and turbulent airflow based on previous studies

Researchers	Laminar Airflow, <i>ml/s</i>	Turbulent Airflow, <i>ml/s</i>
Keyhani et al.[26]	< 200	> 200
Lee et al. [28]	< 250	> 250
Zubair et al. [25]	< 250	> 250
Riazuddin et al. [9]	< 250	> 250
K. Smith [20]	< 250	> 250
Wen et al. [8]	< 400	> 400

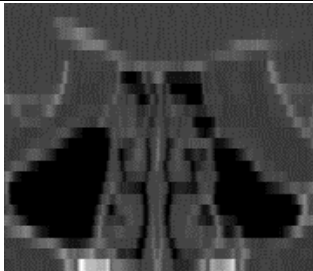
The mass flow rate utilized in this study ranges between 50-400ml/s, 50-200ml/s were used for laminar airflow simulation while for turbulent airflow simulation, the mass flow rate used were 300ml/s and 400ml/s. To account for the existences of turbulence, the Reynold average Navier-Stokes (RANS) equations were implemented, to solve the turbulent flow with low Reynolds k- $\omega$  model [3], [29]. This model had been proven by Chen et al. in his research to be appropriate to describe the low levels internal swirling in the nasal cavity, and it was further experimentally validated by Wen et al. and Mylayarapu et al. for its applicability in turbulent flow case [3], [29], [30]. The shear stress transport option with transitional flow treatment was also selected to capture complex laminar-transitional turbulent flow. Turbulent density and turbulent viscosity ratio were both set as 5%, a value typically for low Reynolds no. case [29].

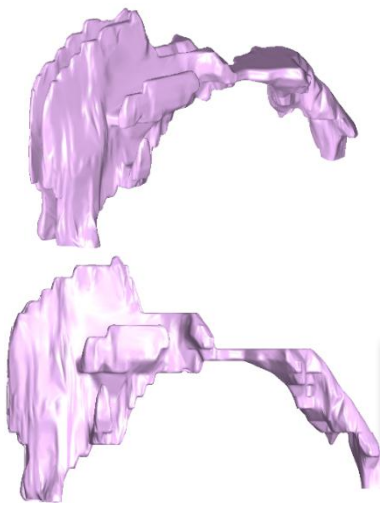
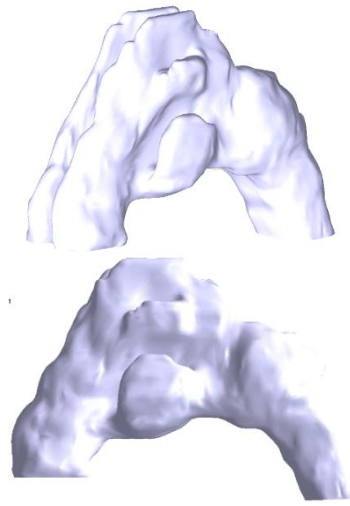
**III. RESULTS AND DISCUSSION**

Results acquired from the female child model were presented and discussed in three major sections. The first section is the geometrical comparison of two nasal cavity models, one of them is the developed female child model, and the second model is the standardized female adult model generated by Lee et al. [15]. In this section, the comparisons were performed via visual observation on the CT scans and the 3D nasal cavity models. The second part of this study was focused on the statistical data comparisons, comparing the general nasal attributes such as nasal width, nasal height and cross-sectional area of three models – female child, male child and standardized female adult. Lastly, the third section involved the comparison of models through various results obtained from the CFD analysis.

The results discussed include pressure drop, average velocity magnitude, velocity contours and velocity streamlines. The geometrical differences of the nasal cavity for female child and standardized female adult are illustrated in Table 2. Clear and good resolution CT scans are very important in this section, to ensure more realistic and precise nasal geometry developed. As a human grow from birth to adulthood, both airway geometry and respiratory condition vary with age.

**Table 2:** CT scans and nasal cavity models of female child and adult nasal cavities

	<b>Female Child</b>	<b>Female Adult</b>
<b>CT scans</b>		

	Female Child	Female Adult
Nasal Cavity Model		

All the airways are present at the time of birth, and their size increases as age progresses [17]. This statement is further clarified by Warren et al., where he stated that age was directly related to the nasal airway size [31]. Hence, based on Table 2, it can be clearly seen that the nasal passageways of female child nasal cavity are thin and narrow as compared to the standardized female adult model. This signifies that only relatively small amount of air is flowing through the nasal cavity of child and thus, resulting oral breathing [32].

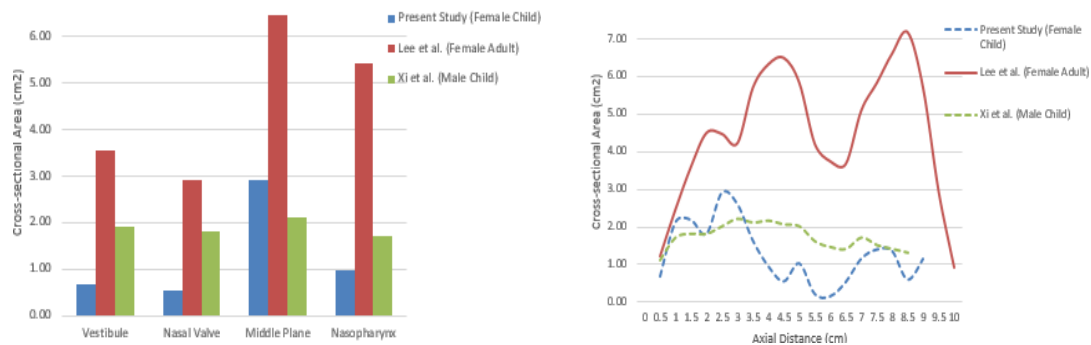
Besides, obvious differences can be noticed in the nasal cavity structures, e.g. superior and posterior turbinate are found from the female child model that is still not fully developed. The superior turbinate is a small structure of the nose, which is hard to be identified by CT scans and is usually neglected in studies because the airflow in this region is considered very small. Moreover, it is absent in more than 80% of the human population [16]. Adult nasal cavity usually consists all three turbinates which are responsible for heat exchange and humidification of the inhaled air [4]. However, in the case of child which air intake is low, the entire air-conditioning function is sufficient to be performed by single turbinate.

Table 3 displays general attributes of the nasal cavities of three models – female child, male child [17] and standardized female adult [15]. Here, the nasal dimensions of the child model can be clearly seen, is a lot smaller than the adult model. Before 11 years old, the nasal length and nasal area were longer and smaller in girls than in boys. However, the situation is vice versa after 11 years old [33]. Therefore, male child nasal cavity is noticed to have shorter length and larger cross-sectional area as compared to female child model. An additional parameter known as nasal index is also introduced and calculated  $((\text{nasal breadth})/(\text{nasal height}) \times 100)$  in this study, to determine the nose shape of an individual – leptorrhine, platyrrhine and mesorrhine. A nasal index below 70 is described as leptorrhine (narrow nose) and when above 85, it is platyrrhine (broad nose). An intermediate index of 70-85 is described as mesorrhine.

**Table 3:** General nasal attributes of various subjects

Authors	Gender	Age	Nasal Length (cm)	Nasal Breadth (cm)	Nasal Height (cm)	Nasal Index	Nasal Area (cm <sup>2</sup> )
Present study	Female	Child	9.09	2.85	5.16	55.23	1.28
Xi et al. [17]	Male	Child	8.60	1.75	3.74	46.79	1.72
Lee et al. [15]	Female	Adult	10.04	3.05	5.52	55.25	4.53

Cross-sectional area along the nasal cavities are presented in Fig 4 for a more thorough comparison of these three models. Based on Fig 4, it can be seen that as compared to adult, the child airways have smaller sized nostrils, shorter turbinate region, thinner and slenderer nasopharynx. Most children below the age of 8 were considered as oral or predominantly nasal breathers. This means that they only utilize 60% or 80% of their nasal airways to perform respiration [34]. Since the air intake into child nasal cavity is relatively low, thus, a short turbinate region is more than enough for air-conditioning purpose and to maintain the normal functioning of child respiratory system.



**Figure 4:** (a) Cross-sectional area at four major region and (b) Comparison of cross-sectional area vs. distance from the anterior tip of nose with previous works

Surprisingly, the nasal valve cross-sectional area was noticed to be the same between the male child and the adult. There are several possible reasons behind the observations above – nasal valve maturation at the early ages or are merely examples of inter-subject variability [35]. Besides, according to Fig 4(b), the cross-sectional area of male child model is found to be larger at the middle region as compared with female child model. This is because male nasal airways experience more dramatic growth during first several years than during other period of life span and hence, resulting a better developed meatus [17]. However, despite of distinctions, a general trend still can be observed on a macro level. For example, a local minimum is found on all three profiles just after the inlet where the nasal valve region exists.

After the nasal valve region, an increase in cross-sectional area profiles is noticed. This is due to the enlargement of the airways to accommodate the olfactory receptors and the turbinate bone projections [8]. Lastly, all three profiles are found to face a sudden decline. This decline was caused by the ending of the turbinate region and simultaneously, the beginning of the nasopharynx region. By referring to Fig 3(b), large pressure drop deviation can be noticed between child and the adult model. Pressure drop, in some studies is also known as breathing resistance. Infants and children have much higher breathing resistance than adults for an identical flow rate and thus, as expected, the pressure drop data for the child situate above the adult. Children grow fast in height and weight before seven and the rate of growth reduces thereafter, so does the growth of nasal airways [36]. It is therefore reasonable that both the male and female child model's pressure drop is higher than the adult.

Apart from that, the numerical results obtained demonstrate a good agreement with results from Xi et al., especially at inhalation flow rate less than 200 ml/s. The slopes of the curves are found to be almost the same for the laminar flow rates ( $<250$  ml/s). However, due to the turbulent flow effect, the curves start to deviate from each other as the flow rate continues to increase. Besides, in the case of female child subject, the curve is much steeper than that of the male child subject. This may be caused by the anatomical differences. To further evaluate the influence of age on nasal cavity, the average velocity magnitude data of varying age groups have also been plotted in Fig 5.

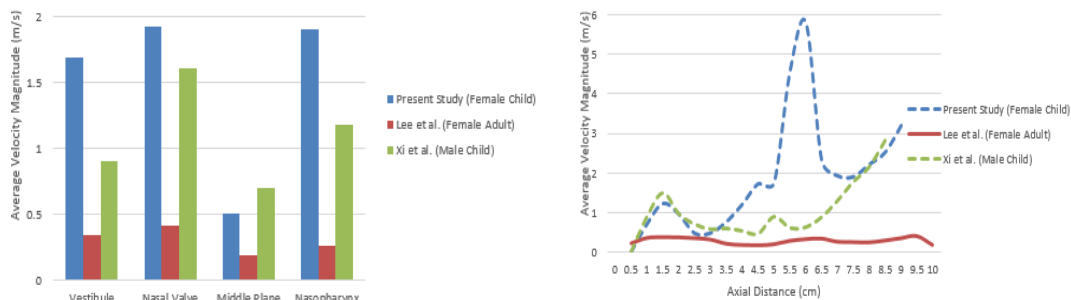


Figure 5: (a) Average velocity magnitudes at four major cross-sections and (b) average velocity profiles comparison along the nasal cavity with previous works

As shown in Fig 5(a), similar pattern can be examined from these three models with the highest velocity resulted from the nasal valve, followed by a sharp decrease at the turbinate region and finally, increase again at the nasopharynx. When entering turbinate region, the air stream is damped and its velocity is further reduced to only 30% of the main flow, in order to distribute airflow towards the olfactory region and at the same time, to protect the olfactory nerve, sensitive area that is directly connected to brain [17].

Aside from similarities, differences can also be clearly detected from Fig 5. For example, child models possess higher average velocity magnitudes as compared to adult. Such significant differences are strongly linked to the variation of cross-sectional

area in Fig 4. A large increment in cross-sectional area of nasal cavity for adult model from 3.0 to 8.5 cm<sup>2</sup> results a drop in the average velocity. Meanwhile, in the case of child models, a sudden and huge reduction in cross-sectional area from 3.0 to 6.0 cm<sup>2</sup> causes the average velocity to increase drastically.

Besides, in the case of female child, high velocity flows are observed in the middle section of the nasal passage in which such sign is not spotted in the male child model. This is due to the narrow meatus regions of the female child in their early ages, before entering adolescent stage [32]. Velocity contours are also developed in this study (Table 4) to clearly illustrate the physical difference of child and adult model as well as the airflow analysis in the nasal cavities. Huge difference can be observed in term of nasal geometry between female adult model and female child model.

**Table 4:** Inspiration velocity contours for mass flow rate of 125 ml/s, at four main cross sections of female child and adult nasal cavity models

Present Study (Female Child)	Cross Section	Lee et al. (Female Adult)
	Vestibule	
	Nasal Valve	
	Middle Plane	
	Nasopharynx	

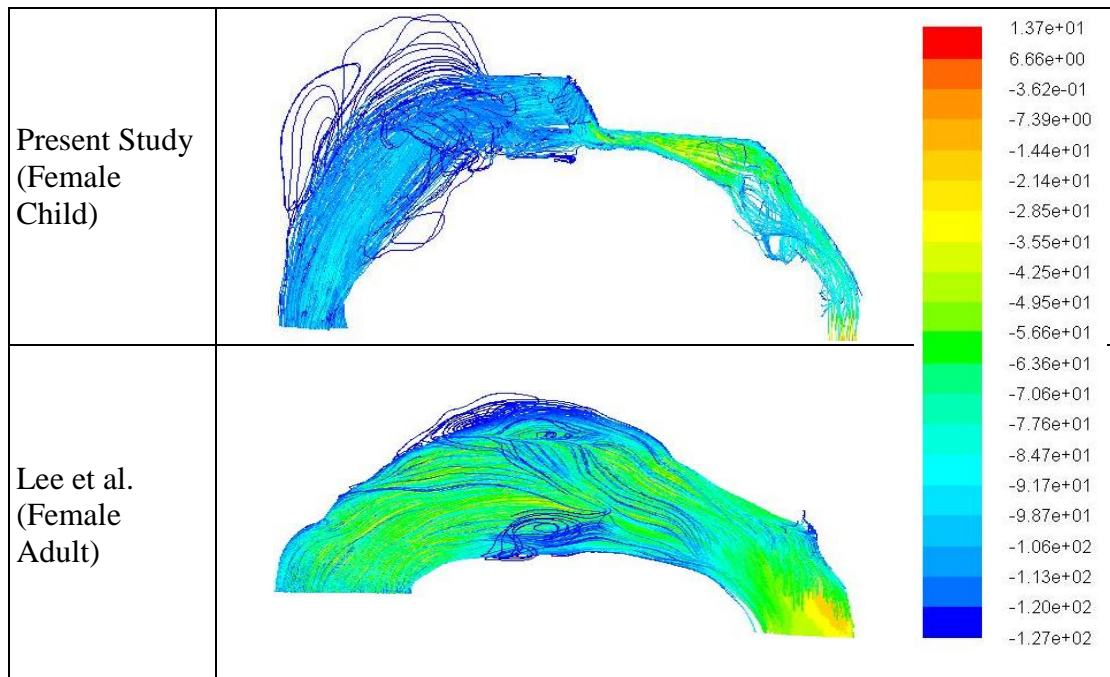
1.37e+01  
6.66e+00  
-3.62e-01  
-7.39e+00  
-1.44e+01  
-2.14e+01  
-2.85e+01  
-3.55e+01  
-4.25e+01  
-4.95e+01  
-5.66e+01  
-6.36e+01  
-7.06e+01  
-7.76e+01  
-8.47e+01  
-9.17e+01  
-9.87e+01  
-1.06e+02  
-1.13e+02  
-1.20e+02  
-1.27e+02

Adult model displays a vestibule, nasal valve and nasopharynx that are more oval in shape, while child model shows an inconsistent shape. Besides, slenderer middle plane is noticed for child as compared to adult model, which demonstrates a rounder shape of meatuses. Apart from geometry difference, the flow field is found more concentrated centrally in child from nasal valve up to middle plane. Meanwhile, in the case of adult, the airflow is well distributed all over the cross-sectional area.

Both nasal resistance and wall shear stress play significant roles in contributing such airflow patterns. In child, nasal resistance and wall shear stress can contribute up to half of the total airways resistance due to the pre-mature geometry of child [8]. The presence of wall shear stress also restricts the flow at the near wall region, establishing dark blue region in the velocity contours. In addition, larger contour area with red, signifying high velocity can always be found in the left cavity in the child model. Left cavity covers only 39% of the entire cross-section, however, right cavity is slightly wider, taking up 61% of the area, and hence, exhibiting high velocity airflow in the left nasal cavity due to area coverage difference [8].

Another approach, velocity vectors and streamlines are also implemented as shown in Table 5 to provide a pictorial view of macro flow features of the air particles throughout the nasal cavity. According to Table 5, vortices can be clearly observed directly behind the nasal valve in the child model, meanwhile in the case of adult model, there are only some weak recirculation occurred instead of visible vortices. This vortex formation is due to the sudden turn of airstream posteriorly, approximately  $90^\circ$  towards the nasopharynx.

**Table 5:** Velocity vectors and streamlines for mass flow rate of 125 ml/s of female child and adult nasal cavity models



This transition coupled with the narrowing geometry establishes the adverse pressure gradient and forces the flow to recirculate, thus, giving rise to vortices. Despite of difference, these two models are also found sharing some similarities. Re-circulatory flow was noticed prominently at the upper roof, the olfactory region of the nasal cavity. This flow feature is considered as desirable as it is a defense mechanism that slows down the airflow and at the same time, avoiding particles whose trajectories are greatly dependent on flow patterns from being deposited onto the sensitive olfactory nerve fibers.

In summary, as compared to other models, the present study model exhibited a narrower and thinner nasal passageway, and also shorter turbinate regions. Despite of this, a general trend was observed for the cross-sectional area and average velocity magnitude profiles of the airways along the axial distance. Pressure drop or breathing resistance of child models was noticed higher than the adult model. In addition, in child, the flow field was observed more concentrated centrally as the airstream is developing. The vortices were also found prominently in the upper olfactory region and just posterior to the nasal valve. These result were considered reasonable as on macro level, the data collected were quite close with the male child model, exactly following the same trend of that model.

#### **IV. CONCLUSION**

To better understand the effect of age on human nasal cavity, the nasal geometry and the airflow characteristics were investigated and compared with available models from the previous studies. The computational nasal cavity model developed based on CT scans of a Malaysian female child exhibited a narrower and thinner nasal passageway, and also turbinate regions with shorter length as compared to other models, male child and female adult model. Despite of this, a general trend was observed on macro level for the cross-sectional area and average velocity magnitude profiles of the airways along the axial distance. Besides, pressure drop of child models was found greater than the adult model as child model possess higher breathing resistance for an identical flow rate. Furthermore, the flow field in child was observed more concentrated centrally as the airstream is progressing. Moreover, the vortices were found primarily in the upper olfactory region and just posterior to the nasal valve. In conclusion, based on the result obtained, age was proven to have influence on human nasal cavity and thus, child model should be studied independently as data acquired from adult model has huge geometrical difference. These findings will be beneficial for various new research opportunities and may be treatment planning of child disease cases in the future.

#### **Acknowledgment**

The authors acknowledge the support provided by RU Grant Universiti Sains Malaysia PAERO/1001/814276 in carrying out this work.

**REFERENCES**

- [1] M. Wolf, S. Naftali, R. C. Schroter, and D. Elad, "Air-conditioning characteristics of the human nose.," *J. Laryngol. Otol.*, vol. 118, no. 2, pp. 87–92, 2004.
- [2] D. Elad, M. Wolf, and T. Keck, "Air-conditioning in the human nasal cavity.," *Respir. Physiol. Neurobiol.*, vol. 163, no. 1–3, pp. 121–7, 2008.
- [3] J. Wen, K. Inthavong, Z. Tian, J. Tu, C. Xue, and C. Li, "Airflow patterns in both sides of a realistic human nasal cavity for laminar and turbulent conditions," *16th Australas. Fluid Mech. Conf.*, no. December, pp. 68–74, 2007.
- [4] F. Chometon, P. Gillieron, and J. Laurent, "Aerodynamics of Nasal Airways with Application to Obstruction," *World Wide Web. http/ ...*, pp. 1–6, 2000.
- [5] N. Geurkink, "Nasal anatomy, physiology, and function," *J. Allergy Clin. Immunol.*, vol. 72, no. 2, pp. 123–128, 1983.
- [6] "a Numerical Study of Airflow Through," 2012.
- [7] K. Hemtiwakorn, N. Phoocharoen, S. Tungjitkusolmun, and C. Pintavirooj, "Nasal Airflow Simulation in Human Using a Computational Fluid Dynamics (Cfd)," *2nd Biomed. Eng. Int. Conf. (BMEiCON 2009)*, no. BMEiCON, pp. 335–338, 2009.
- [8] J. Wen, K. Inthavong, J. Tu, and S. Wang, "Numerical simulations for detailed airflow dynamics in a human nasal cavity.," *Respir. Physiol. Neurobiol.*, vol. 161, no. 2, pp. 125–135, 2008.
- [9] V. N. Riazuddin, M. Zubair, M. Z. Abdullah, R. Ismail, I. L. Shuaib, S. A. Hamid, and K. A. Ahmad, "Numerical study of inspiratory and expiratory flow in a human nasal cavity," *J. Med. Biol. Eng.*, vol. 31, no. 3, pp. 201–206, 2011.
- [10] D. J. Doorly, D. J. Taylor, a M. Gambaruto, R. C. Schroter, and N. Tolley, "Nasal architecture: form and flow," *Philos. Trans. R. Soc. Ser. A, Math. Phys. Eng. Sci.*, vol. 366, no. 1879, pp. 3225–3246, 2008.
- [11] D. J. Doorly, D. J. Taylor, and R. C. Schroter, "Mechanics of airflow in the human nasal airways," *Respir. Physiol. Neurobiol.*, vol. 163, no. 1–3, pp. 100–110, 2008.
- [12] G. Xiong, J. Zhan, K. Zuo, J. Li, L. Rong, and G. Xu, "Numerical flow simulation in the post-endoscopic sinus surgery nasal cavity," *Med. Biol. Eng. Comput.*, vol. 46, no. 11, pp. 1161–1167, 2008.
- [13] J. Lee, Y. Na, S. Kim, and S. Chung, "Respiratory Physiology & Neurobiology Unsteady flow characteristics through a human nasal airway," vol. 172, pp. 136–146, 2010.
- [14] D. J. Taylor, D. J. Doorly, and R. C. Schroter, "Inflow boundary profile prescription for numerical simulation of nasal airflow," *J. R. Soc. Interface*, vol. 7, no. September 2009, pp. 515–527, 2010.

- [15] C. F. Lee, M. Z. Abdullah, K. A. Ahmad, and I. L. Shuaib, "Standardization of Malaysian Adult Female Nasal Cavity," vol. 2013, 2013.
- [16] C. Croce, R. Fodil, M. Durand, G. Sbirlea-Apiou, G. Caillibotte, J. F. Papon, J. R. Blondeau, A. Coste, D. Isabey, and B. Louis, "In Vitro Experiments and Numerical Simulations of Airflow in Realistic Nasal Airway Geometry," *Ann. Biomed. Eng.*, vol. 34, no. 6, pp. 997–1007, 2006.
- [17] J. Xi, X. Si, J. Won, and A. Berlinski, "Simulation of airflow and aerosol deposition in the nasal cavity of a 5-year-old child," *J. Aerosol Sci.*, vol. 42, no. 3, pp. 156–173, 2011.
- [18] S. C. Leong, X. B. Chen, H. P. Lee, and D. Y. Wang, "A review of the implications of computational fluid dynamic studies on nasal airflow and physiology," *Rhinology*, vol. 48, no. 2, pp. 139–145, 2010.
- [19] C. F. Lee, K. A. Ahmad, R. Ismail, and S. A. Hamid, "Mucous layer effects towards nasal airflow," *2012 Int. Conf. Biomed. Eng. ICoBE 2012*, no. February, pp. 276–279, 2012.
- [20] B. J. S. Nc and K. Smith, "CFD Analysis of Pressure and Flow Characteristics of the Human Nose by."
- [21] C. Kleinstreuer and Z. Zhang, "Airflow and Particle Transport in the Human Respiratory System," *Annu. Rev. Fluid Mech.*, vol. 42, no. 1, pp. 301–334, 2010.
- [22] I. Weinhold and G. Mlynski, "Numerical simulation of airflow in the human nose," *Eur. Arch. Oto-Rhino-Laryngology*, vol. 261, no. 8, pp. 452–455, 2004.
- [23] T. van Reimersdahl, I. Hörschler, a. Gerndt, T. Kuhlen, M. Meinke, G. Schlöndorff, W. Schröder, and C. H. Bischof, "Airflow simulation inside a model of the human nasal cavity in a virtual reality based rhinological operation planning system," *Int. Congr. Ser.*, vol. 1230, pp. 87–92, 2001.
- [24] H. Shi, C. Kleinstreuer, and Z. Zhang, "Laminar airflow and nanoparticle or vapor deposition in a human nasal cavity model.," *J. Biomech. Eng.*, vol. 128, no. 5, pp. 697–706, 2006.
- [25] M. Zubair, V. N. Nazira, M. Z. Zulkifly, R. Ismail, I. L. Shuaib, S. A. Hamid, and K. A. Ahmad, "Airflow inside the nasal cavity: visualization using computational fluid dynamics," *Asian Biomed.*, vol. 4, no. 4, pp. 657–661, 2010.
- [26] K. Keyhani, P. W. Scherer, and M. M. Mozell, "A numerical model of nasal odorant transport for the analysis of human olfaction.," *J. Theor. Biol.*, vol. 186, no. 3, pp. 279–301, 1997.
- [27] G. J. M. Garcia, N. Bailie, D. a Martins, and J. S. Kimbell, "Atrophic rhinitis: a CFD study of air conditioning in the nasal cavity.," *J. Appl. Physiol.*, vol. 103, no. 3, pp. 1082–1092, 2007.
- [28] C. F. Lee, M. Z. Abdullah, K. A. Ahmad, and I. L. Shuaib, "Analytical Comparisons of Standardized Nasal Cavity," *J. Med. Imaging Heal. Informatics*,

- vol. 4, no. 1, pp. 14–20, 2014.
- [29] X. B. Chen, H. P. Lee, V. F. H. Chong, and D. Y. Wang, “Numerical simulation for nasal flow with partial inferior turbinatomy - A turbulent model,” *2nd Int. Conf. Biomed. Pharm. Eng. ICBPE 2009 - Conf. Proc.*, no. 978, pp. 1–3, 2009.
- [30] G. Mylavarapu, S. Murugappan, M. Mihaescu, M. Kalra, S. Khosla, and E. Gutmark, “Validation of computational fluid dynamics methodology used for human upper airway flow simulations,” vol. 42, pp. 1553–1559, 2009.
- [31] K. H. Cheng, Y. S. Cheng, H. C. Yeh, R. A. Guilmette, S. Q. Simpson, Y. H. Yang, and D. L. Swift, “In vivo measurements of nasal airway dimensions and ultrafine aerosol deposition in the human nasal and oral airways,” *J. Aerosol Sci.*, vol. 27, no. 5, pp. 785–801, 1996.
- [32] S. Shanker, H. W. Fields, F. . Beck, P. . Vig, and K. W. . Vig, “A longitudinal assessment of upper respiratory function and dentofacial morphology in 8- to 12-year-old children,” *Semin. Orthod.*, vol. 10, no. 1, pp. 45–53, 2004.
- [33] Y. Miyamoto, K. Takeuchi, and Y. Majima, “Measurement of nasal patency by acoustic rhinometry in Japanese school children,” *Auris Nasus Larynx*, vol. 36, no. 4, pp. 406–410, 2009.
- [34] P. S. VIG and D. J. ZAJAC, “Age and gender effects on nasal respiratory function in normal subjects,” *The Cleft palate-craniofacial journal : official publication of the American Cleft Palate-Craniofacial Association*, vol. 30, no. 3, pp. 279–84, 1993.
- [35] K. Zhao, P. W. Scherer, S. A. Hajiloo, and P. Dalton, “Effect of anatomy on human nasal air flow and odorant transport patterns: Implications for olfaction,” *Chem. Senses*, vol. 29, no. 5, pp. 365–379, 2004.
- [36] K. Jost, N. Lenherr, F. Singer, S. M. Schulzke, U. Frey, P. Latzin, S. Yammine, and S. Y. Kerstin Jost, Nina Lenherr, Florian Singer, Sven Schulzke, Urs Frey, Philipp Latzin, “Changes in breathing pattern upon 100% oxygen in children at early school age,” *Respir Physiol Neurobiol*, vol. accepted, pp. 9–15, 2016.